Stoten, D. P., Yamaguchi, T., & Yamashita, Y. (2016). Dynamically Substructured System Testing for Railway Vehicle Pantographs. Journal of Physics: Conference Series, 744(1), [012204]. DOI: 10.1088/1742-6596/744/1/012204

Dynamically Substructured System Testing for Railway Vehicle Pantographs

2016 J. Phys.: Conf. Ser. 744 012204

(http://iopscience.iop.org/1742-6596/744/1/012204)

Dynamically Substructured System Testing for Railway Vehicle Pantographs

D P Stoten[1], T Yamaguchi[1,2] and Y Yamashita[3]

[1]Advanced Control and Test Laboratory (ACTLab), Department of Mechanical Engineering, University of Bristol, Bristol BS8 1TR, UK

[2]Running Gear Laboratory, Vehicle Structure Technology Division, Railway Technical Research Institute, Tokyo 185-8540, Japan

[3]Current Collection Laboratory, Railway Dynamics Division, Railway Technical Research Institute, Tokyo 185-8540, Japan

E-mail: d.p.stoten@bristol.ac.uk

Abstract. The overall objective of this paper is to establish a dynamically substructured system (DSS) testing approach for railway vehicle pantographs. In this approach a pilot study quasi-pantograph (QP) is tested within a laboratory environment, where the catenary wire, contact wire and catenary support (abbreviated as 'catenary' in this paper) are modelled as a numerical substructure. This is simulated in real time and in parallel with the operation of the physical substructure, *i.e.* the QP rig itself. The entire DSS is driven by parametric excitation within the catenary model, whilst the numerical and physical substructures are synchronised at their interface via the DSS control technique of [1]. Simulation and physical experimental investigations of the pilot QP rig, constructed within the Advanced Control and Test Laboratory at the University of Bristol, UK, demonstrate the efficacy of the method when subjected to parametric variations, unknown parameter values and parametric excitation.

1. Introduction

In recent years, the concept of testing an engineering system using a combination of physical and real-time numerical substructures has become a viable alternative to testing entirely physical or entirely numerical systems. Underlying reasons for this move include problems with (i) the cost and viability of full-size physical testing of an entire system; (ii) the validation of numerical methods when the dynamics of critical elements are unknown or uncertain in terms of parameters and structure; (iii) similitude problems associated with nonlinear, scaled physical model testing. In this new approach, the combination of system elements can include more than one substructure of each type - physical or numerical. However, without loss of generality, in this paper we restrict the investigation to just one substructure of each type. In addition, the combination of substructures may be excited by external or internal disturbances of one form or another. Again without loss of generality, we examine a specific problem where the excitation is confined to the numerical substructure, in the form of a parametric excitation.

One common method for the implementation of substructured system testing is the hybrid scheme (HS). This is also variously known as hybrid simulation or pseudo-dynamic testing [2], and was originally formulated by [3], [4] for testing large structural systems. Since the 1990s, HS developments have been extensively used for substructured testing within the fields of structural,

earthquake, civil and mechanical engineering. Very often the scheme has been given the misnomer of hardware-in-the-loop simulation (HiLS). However, the original purpose of HiLS [5], [6] was quite different to that of HS and this has led to some confusion over the fundamental objectives and the basis of design for each method. It is possible that this misunderstanding has been further exacerbated via the more recent dynamically substructured system (DSS) approach [1]. Thus, in [7], one of the main objectives was to remove any confusion between the HiLS, HS and DSS testing methods. General observations from [7] are:

(i) HiLS is primarily a method for testing a physical controller design, Σ_P, against an embedded numerical simulation of the controlled plant, Σ_N, within a closed-loop configuration; see figure 1. Therefore, in its original form, HiLS is not a suitable method for solving general substructured test problems.

(ii) HS combines a physical substructure (or component), Σ_P , with a real-time numerical substructure, Σ_N , in order to emulate a given open-loop system (*i.e.* plant), Σ_E; see figure 2. Hence, HS is a *bona fide* in-series substructure testing method, with an entirely different conceptualisation to that of HiLS. Synthesis of the HS is relatively straightforward, essentially requiring exact cancellation of the actuator (transfer system) dynamics Σ_{TS}, via a compensator Σ_{Cr}, in order to ensure that the response of Σ_P, (y_P), matches that of Σ_N, (y_N). Therefore HS suffers from the stringent requirements that the transfer system dynamics are (ideally) known precisely and also invertible. In addition, the method aims to ensure that the closed-loop dynamics shown in figure 2 are the same as those of an emulated system, Σ_E. As a consequence, a Σ_E with low damping (*e.g.* a structural system) can quite easily result in an HS which exhibits poor relative stability, or even instability, given imprecise knowledge of the underlying dynamics. This stability problem is compounded by any pure delays in the system, typically due to digital computational elements within Σ_{Cr}.

(iii) DSS has exactly the same objective as for HS; however it is achieved via the parallel substructure testing method shown in figure 3. Although the synthesis procedure for Σ_C is more involved than that for Σ_{Cr}, the closed-loop dynamics within the DSS structure can be designed to have a high level of relative stability - and hence robustness - in the face of parameter unknowns and pure delay terms. An analysis of the overall DSS dynamics shows that the characteristic polynomial of the required Σ_E is quite distinct from that of the closed-loop error (synchronisation) dynamics that are highlighted in figure 3; [7]. Hence, by design, a Σ_E with low damping will not result in a DSS with low levels of relative stability.

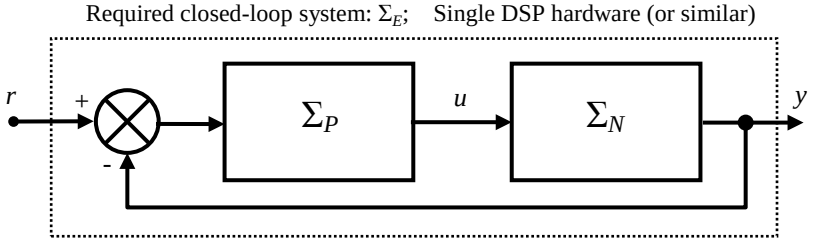

Figure 1 Hardware-in-the-loop simulation: *r*: reference; *u*: control; *y*: output; Σ_E: emulated closed-loop control system; Σ_P: controller; Σ_N: embedded plant simulation

Given the inherent robustness of the DSS design, the principal objective of this paper is to investigate the viability of the method for testing substructured railway vehicle pantographs. This includes the dynamic analysis of a typical DSS pantograph system and the experimental testing of a quasi-pantograph (QP) pilot study rig that has been constructed in the Advanced Control and Test Laboratory (ACTLab) at the University of Bristol, UK. Purely physical catenary-pantograph dynamic testing facilities already exist and continue to provide valuable information, but they are often restricted in operation. For example, a sophisticated testing facility at the Railway Technical Research Institute (RTRI) facility in Tokyo, Japan, consists of a tracked vehicle, pantograph and catenary. However, the vehicle is limited to a maximum speed of 200 km/h and runs on a track of

maximum length 60 m. Smaller, stationary test facilities use an exciter in place of the physical catenary, but they do not allow the possibility of true dynamic interaction at the point of contact between the pantograph and exciter. For these reasons, DSS testing has become an attractive alternative, allowing the possibility of virtual high-speed testing over an extended track length, together with realistic dynamical interactions at the point of contact between the pantograph and catenary.

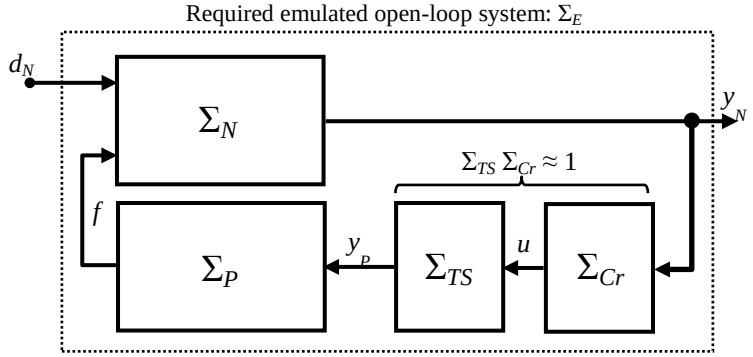

Figure 2 Hybrid simulation: d_N: excitation; u: control; y_N: numerical output; y_P: physical output; f: interaction constraint; Σ_E: emulated system; Σ_P: physical substructure; Σ_N: numerical substructure; Σ_{TS}: transfer system; Σ_{Cr}: HS compensator

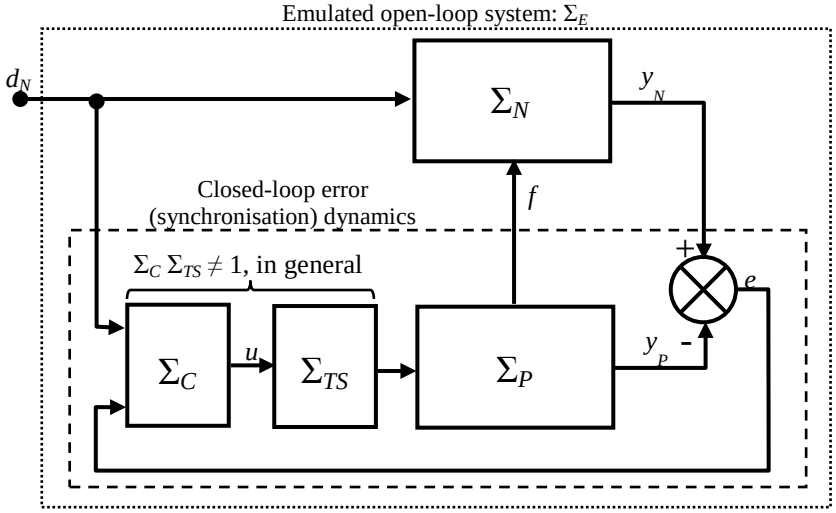

Figure 3 Dynamically substructured system: d_N: excitation; u: control; y_N: numerical output; y_P: physical output; f: interaction constraint; e: error; Σ_E: emulated open-loop system; Σ_P: physical substructure; Σ_N: numerical substructure; Σ_{TS}: transfer system; Σ_C: DSS controller

The remainder of this paper is organised as follows. In §2 a pantograph-catenary model is described, together with the associated QP rig and its control systems. The corresponding DSS developments are then described in §3, together with the derivation of the DSS controller itself. Stability analysis of the DSS controller design follows in §4, focusing on the effects of parameter variations and pure delays due to discrete-time computational elements in Σ_C and Σ_{TS}. Results from experimental investigations conducted on the QP rig are presented in §5. Finally, the main conclusions to this work are presented in §6, together with comments on future research in this field.

2. Pantograph/catenary model and the QP pilot study test rig

Schematics of the pantograph-catenary system are shown in figure 4. A basic arrangement of the power car, pantograph and catenary (with regularly spaced supports) is shown in figure 4(a); the car is assumed to be travelling at a constant velocity, v. The corresponding catenary stiffness in the vertical direction, k_1, is shown in figure 4(b), with the time axis calibrated for a car velocity $v = 100$ km/h. A simplified and linearised *m-k-c* model of the vertical motion dynamics of this

system is shown in figure 4(c), where parameters are nominally constant, apart from k_1, and that contact between the catenary (with local mass m_1) and the pantograph (mass m_2) is maintained. Associated damping characteristics of the catenary and pantograph are represented by the viscous friction coefficients c_1 and c_2, respectively. The vertical motion of the point of contact between the catenary and pantograph is y and the corresponding motions of the catenary support and vehicle body are d_1 and d_2, respectively. In what follows, both d_1 and d_2 are assumed to be zero and excitation of the system will be provided by an internal parametric variation due to continuous change in the catenary stiffness, k_1.

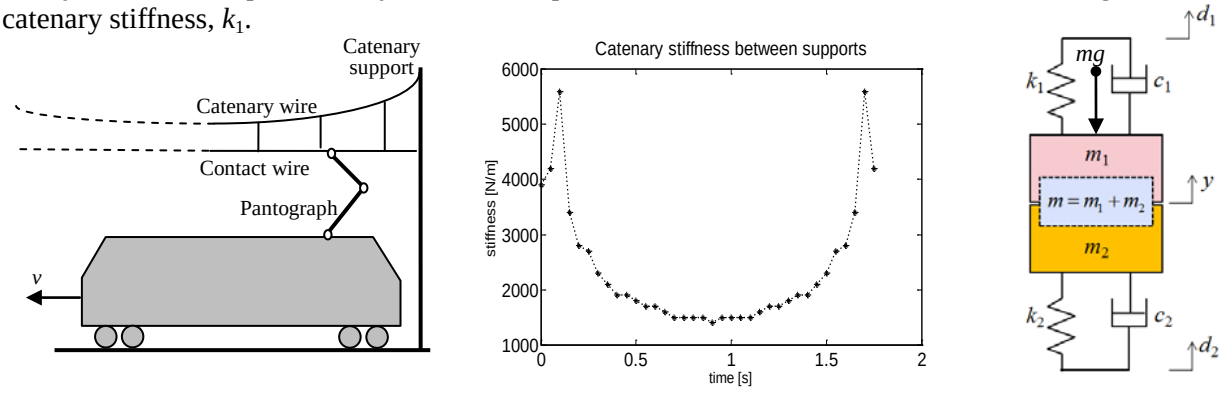

(a) (b) (c)

Figure 4 Pantograph-catenary schematics; the 'catenary' consists of the catenary wire, contact wire and supports (a) Basic arrangement (b) Catenary stiffness (time axis calibrated for v = 100 km/h) (c) Linearised *m-k-c* model

Figure 5 shows three of the four components of the proposed QP DSS; the fourth component is the DSS controller, Σ_C, which is yet to be designed.

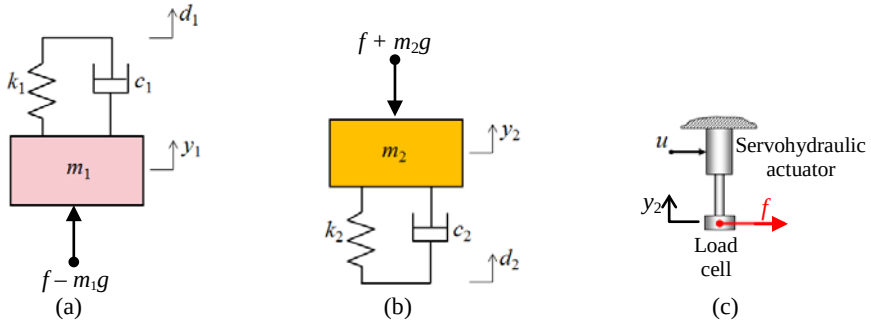

(a) (b) (c)

Figure 5 QP DSS: (a) Numerical substructure Σ_N (b) Physical substructure Σ_P (c) Transfer system Σ_{TS}

Σ_{TS} in figure 5(c) consists of an Instron 25kN, ±130mm stroke servohydraulic actuator with hydrostatic bearings, complete with a load cell for the measurement of the force, f, and a linear variable differential transformer (LVDT) for the measurement of the displacement, y_2. In addition, Σ_{TS} incorporates a fixed gain inner-loop controller for y_2, implemented via an Instron 8800 digital system. The Σ_{TS} and Σ_P hardware, apart from the 8800 system, is shown in figure 6.

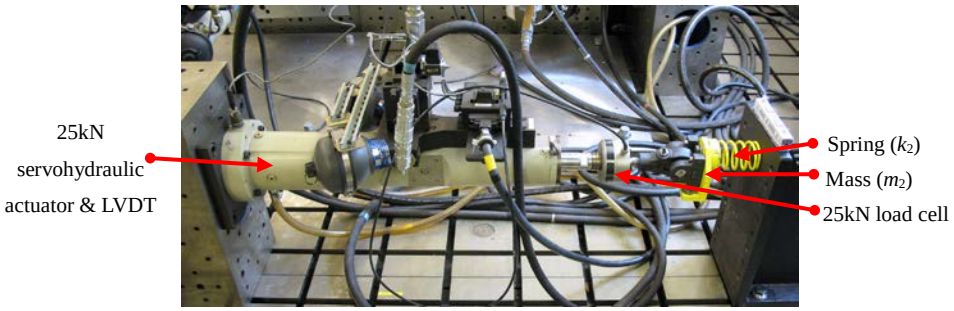

Figure 6 Principle elements of the Σ_{TS} and Σ_P subsystems (the Instron 8800 inner-loop controller is not shown)

3. DSS substructure models and linear substructuring controller design

3.1. DSS substructure models

Although Σ_E is not used in the development of the DSS substructures, or in the synthesis of the DSS controller, or in the implementation of the method, its formulation is useful in providing an idealised response for the purposes of comparison. Thus, in figure 4(c), the end deflections d_1 and d_2 are assumed to be zero and the variable catenary stiffness provides an internal parametric excitation to the system. Writing $k_1 = k_1^* + k_{1t}$, where k_1^* is a nominal value of the stiffness and k_{1t} is an instantaneous variation about the nominal (see figure 4(b)), together with $m = m_1 + m_2$, $k = k_1^* + k_2$ and $c = c_1 + c_2$, the equation of motion of Σ_E is $-[(k_1^* + k_{1t})y + k_2 y] - c\dot{y} - mg = m\ddot{y}$. Hence, in the Laplace domain:

$$\Sigma_E: \; y = -\left(\frac{1/m}{s^2 + (c/m)s + k/m}\right) d_e - \left(\frac{1}{s^2 + (c/m)s + k/m}\right) g \tag{1}$$

where the parametric excitation due to catenary stiffness variations is $d_e = k_{1t}\, y$. Similarly for Σ_N, figure 5(a) yields $-[(k_1^* + k_{1t})]y_1 - c_1\dot{y}_1 - m_1 g + f = m_1\ddot{y}_1$, so that:

$$\Sigma_N: \; y_1 = -\left(\frac{1/m_1}{s^2 + (c_1/m_1)s + k_1^*/m_1}\right) d_{e1} - \left(\frac{1}{s^2 + (c_1/m_1)s + k_1^*/m_1}\right) g + \left(\frac{1/m_1}{s^2 + (c_1/m_1)s + k_1^*/m_1}\right) f \tag{2}$$

where $d_{e1} = k_{1t}\, y_1$. Regarding Σ_P, figure 5(b) yields $-k_2 y_2 - c_2\dot{y}_2 - m_2 g - f = m_2\ddot{y}_2$, so that:

$$\Sigma_P: \; y_2 = -\left(\frac{1/m_2}{s^2 + (c_2/m_2)s + k_2/m_2}\right)(m_2 g + f) \tag{3}$$

Finally, experimental evidence shows that Σ_{TS} can be approximated as a first-order transfer function over the frequency range of interest, *i.e.* in figure 5(c):

$$\Sigma_{TS}: \; y_2 \approx \left(\frac{a}{s+a}\right) u \tag{4}$$

where the numerator and denominator adopt the same parameter, a, as a result of combining the integral form of the actuator dynamics with the 8800 system proportional controller of gain k_p.

3.2. Linear substructure controller synthesis

Using equations (1)-(4), a straightforward extension to the linear substructure controller (LSC), first proposed by [1], is now synthesised for the QP DSS rig. Full analysis and synthesis details of the general LSC development can be found in [1], [7]. LSC has the following two degree-of-freedom structure:

$$u = K_{1e} d_{e1'} + K_e e \tag{5}$$

where K_{1e} is a feedforward transfer function defined in equation (8) below, K_e is a feedback element (often a simple proportional term), $d_{e1'} = d_{e1} + mg$ is the modified parametric excitation that appears in equations (6) and (7) below and $e = y_1 - y_2$ is the DSS synchronisation error. Manipulation of equations (1)-(4) yields the following expression for e in terms of $d_{e1'}$ and u:

$$e = -G_{Ne} d_{e1'} - G_u u \; ; \; G_{Ne} = \left(\frac{1/m_1}{s^2 + (c_1/m_1)s + k_1^*/m_1}\right) \; ; \; G_u = \left(\frac{[m/m_1][s^2 + (c/m)s + k/m]}{s^2 + (c_1/m_1)s + k_1^*/m_1}\right)\left(\frac{a}{s+a}\right) \tag{6}$$

The corresponding closed-loop error dynamics are therefore determined from equations (5) and (6):

$$e = -\left(\frac{G_{Ne} + G_u K_{1e}}{1 + G_u K_e}\right) d_{e1'} \tag{7}$$

Hence, in order to ensure that $e \to 0$, the following solution for the LSC feedforward term is proposed:

$$K_{1e} = -G_{Ne} / G_u \tag{8}$$

and to provide closed-loop robustness, the feedback term K_e can be determined via classic design techniques (*e.g.* the roots' loci method) using the closed-loop characteristic equation (CLCE):

$$1 + G_u K_e = 0 \tag{9}$$

A schematic arrangement of the complete DSS is shown in figure 7.

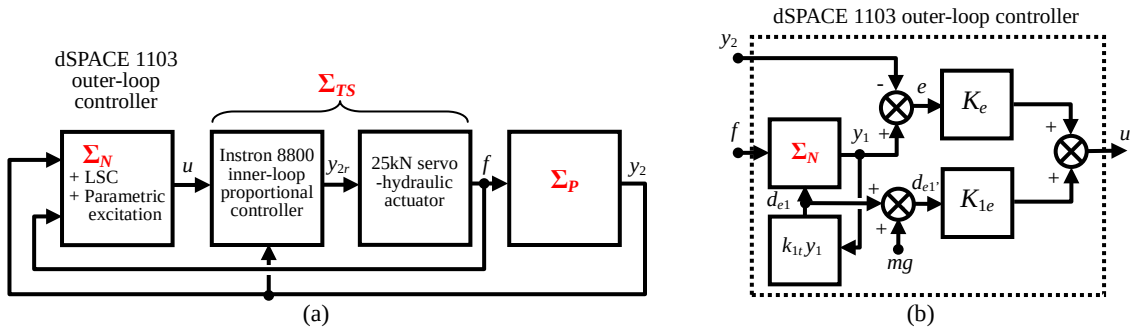

Figure 7 (a) Block schematic diagram of the DSS (b) Detail showing the dSPACE outer-loop controller

3.3. Design for specific parameter values

The following nominal parameter values were used in the emulated system and DSS substructures:

m_1 = 100 kg; m_2 = 7.86 kg; m = 107.9 kg; c_1 = 500 Ns/m, c_2 = 23.95 Ns/m; c = 524.0 kg;
k_1^* = 3.0 kN/m; k_2 = 25.1 kN/m; k = 28.1 kN/m; k_p = 15 dB (≡ 5.623); a = 42.4 s^{-1}; v = 100 km/h

which are used to determine the LSC controller via standard, classical control engineering techniques. From (6):

$$G_{Ne} = \left(\frac{0.01}{s^2+5s+30}\right);\ G_u = 1.079\left(\frac{s^2+4.856s+260.4}{s^2+5s+30}\right)\left(\frac{42.4}{s+42.4}\right) \tag{10}$$

so that the LSC feedforward term is determined from equation (8) as:

$$K_{1e} = -2.187\times10^{-4}\left(\frac{s+42.4}{s^2+4.856s+260.4}\right) \tag{11}$$

yielding the Bode plot of figure 8(a), which shows a resonant frequency of ~15.9 rad/s together with a -20 dB/dec high frequency roll-off.

A proportional control design for the LSC feedback term, K_e, is determined via the roots' loci method. From equation (9), the corresponding standard form of the CLCE is:

$$1+45.75K_e\left(\frac{s^2+4.856s+260.4}{(s^2+5s+30)(s+42.4)}\right)=0 \tag{12}$$

which generates the roots' loci plot of figure 8(b). This shows that the system is unconditionally stable for $K_e \geq 0$; arbitrarily, a nominal value was chosen as $K_e = 2$, corresponding to dominant CLCE roots at $s \approx -1.86 \pm j13.5$. In practice, it was not necessary to improve closed-loop damping of the error dynamics, via the addition of any derivative terms within K_e, for example.

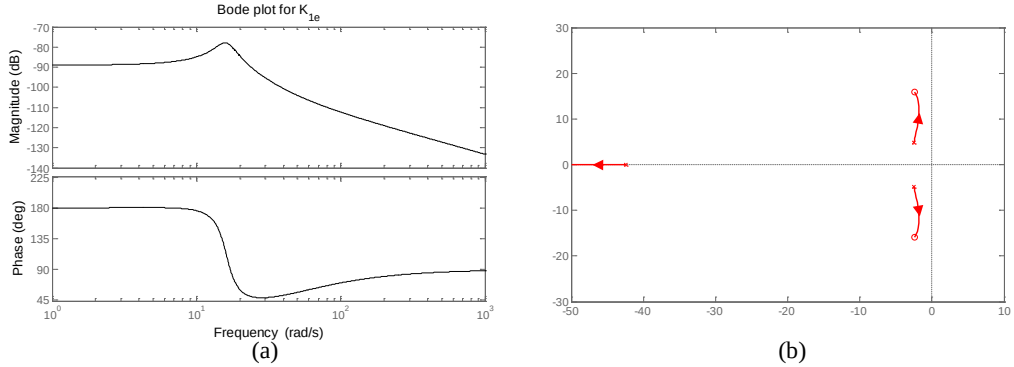

Figure 8 (a) Bode plot for the LSC feedforward term, K_{1e}; (b) Roots' loci of $1 + G_u K_e = 0$ with varying gain $K_e \geq 0$

4. DSS stability analysis with and without a pure delay in the transfer system, Σ_{TS}

4.1. Stability without a pure delay in Σ_{TS}

Stability and robustness of the DSS system to changes in the parameters within Σ_P and Σ_{TS} - which are considered to be unknown and cannot be incorporated into the DSS design - can be confirmed via

simple classical techniques such as the roots' loci method. Note that changes in numerical parameters *are* assumed to be known and can be included in the design of stable DSS via suitable synthesis of the LSC. For example, rewriting equation (9) in order to analyse the effects of varying $m_1 \geq 0$ in Σ_P leads to the following CLCE:

$$1+G_uK_e = 1+(amK_e/m_1)\left(\frac{s^2+(c/m)s+k/m}{s^2+(c_1/m_1)s+k_1^*/m_1}\right)\left(\frac{1}{s+a}\right)=0$$

$$\textit{i.e.}\quad 1+\left(\frac{c_1+m_2aK_e}{m_1}\right)\left(\frac{s^2+((c_1a+caK_e+k_1^*)/(c_1+m_2aK_e))s+(kaK_e+k_1^*a)/(c_1+m_2aK_e)}{s^2(s+a(1+K_e))}\right)=0$$

Substituting all nominal parameter values, apart from m_1, into the above expression gives:

$$1+\left(\frac{835.3}{m_1}\right)\left(\frac{s^2+82.17s+3005}{s^2(s+127.2)}\right)=0 \qquad (13)$$

resulting in the roots' loci, with varying parameter $(1/m_1) \geq 0$, of figure 9(a). Consequently, the closed loop system is unconditionally stable for finite m_1, becoming marginally unstable in the hypothetical case $m_1 \rightarrow \infty$. In a similar manner, investigations show that variations in the physical parameters $\{K_e, m_1, k_1^*\}$ lead to unconditional stability, whereas variations in $\{k_p, c_1\}$ lead to conditional stability. For example, consider the effect of varying k_p, which is tantamount to varying the transfer system coefficient, a. That is, when k_p is described in normal units (*i.e.* not in dB) the linear relationship between the two parameters is $a = (42.4/5.623)k_p = 7.541k_p$. Rewriting equation (9) in order to analyse the effects of varying a within Σ_{TS} results in the following CLCE:

$$1+a\left(\frac{m_1+mK_e}{m_1}\right)\left(\frac{s^2+((c_1+cK_e)/(m_1+mK_e))s+(k_1^*+kK_e)/(m_1+mK_e)}{s(s^2+(c_1/m_1)s+(k_1^*/m_1))}\right)=0$$

so that substitution of the nominal parameter values, apart from a, yields:

$$1+3.158a\left(\frac{s^2+4.902s+187.5}{s(s^2+5s+30)}\right)=0 \qquad (14)$$

which generates the loci shown in figure 9(b), indicating that instability occurs if $0.375 < a < 8.23$.

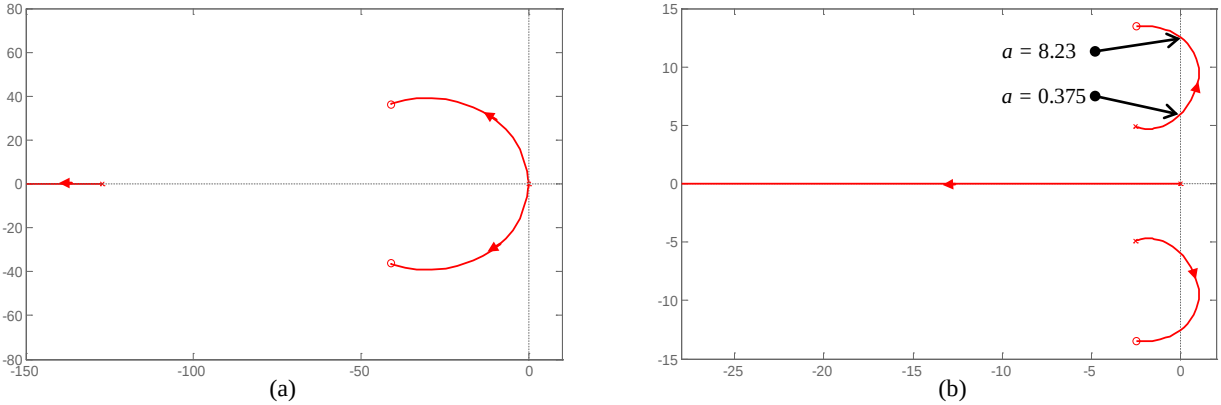

(a) (b)

Figure 9 (a) Roots' loci plot of $1 + G_uK_e = 0$ in equation (13), with varying parameter $(1/m_1) \geq 0$
(b) Roots' loci plot of $1 + G_uK_e = 0$ in equation (14), with varying parameter $a \geq 0$

4.2. Stability with a pure delay in Σ_{TS}

Pure delays can exist within a DSS and for the QP rig this problem occurs within discrete-time elements of the inner-loop 8800 controller, the dSPACE outer-loop LSC controller and also within data acquisition/filtering elements of both controllers. System identification of these components yields an aggregate pure delay $\tau \approx 0.003$ s. Hence, the purpose of this section is to provide a frequency domain investigation of the effect that this delay has on DSS stability.

Incorporating the pure delay into Σ_{TS} results in the following open-loop transfer function, H, within the closed-loop error dynamics:

$$H = K_e G_u e^{-\tau s} = K_e \left(\frac{ms^2 + cs + k}{m_1 s^2 + c_1 s + k_1^*} \right) \left(\frac{a}{s+a} \right) e^{-\tau s} \tag{15}$$

$$H(j\omega) = K_e \left(\frac{(k - m\omega^2) + cj\omega}{(k_1^* - m_1\omega^2) + c_1 j\omega} \right) \left(\frac{a}{a + j\omega} \right) e^{-\tau j\omega} \Rightarrow \left\{ \begin{array}{c} |H(j\omega)| = aK_e \sqrt{\frac{(k - m\omega^2)^2 + c^2\omega^2}{(k_1^* - m_1\omega^2)^2 + c_1^2\omega^2}} \cdot \frac{1}{\sqrt{a^2 + \omega^2}} \\ \angle\{H(j\omega)\} = \tan^{-1}\left(\frac{c\omega}{k - m\omega^2} \right) - \tan^{-1}\left(\frac{c_1\omega}{k_1^* - m_1\omega^2} \right) - \tan^{-1}\left(\frac{\omega}{a} \right) - \tau\omega \end{array} \right\} \tag{16}$$

Plots of $|H(j\omega)|$ and $\angle\{H(j\omega)\}$ from (16) are shown in figure 10, where a family of curves is presented for increments in K_e of 0.5 over the range (0.5, 10) together with increments in τ of 0.001 s over the range (0, 0.020) s. For a given case, the corresponding condition for the onset of stability can be obtained via application of the simplified Nyquist criterion: $|H(j\omega)| = 1$ when $\angle\{H(j\omega)\} = -\pi$, [7]. For example, taking the nominal value of τ = 0.003 s, the frequency at which the phase reaches $-\pi$ rads is ~550 rad/s, so that the K_e = 10 curve (say) can be increased by a factor of approximately 1/0.83 ≈ 1.20 before the onset of instability occurs. Hence the limiting gain for instability when τ = 0.003 s is $K_e \approx 12.0$.

A second example considers the maximum allowable delay for the nominal case K_e = 2. Thus, in figure (10), the magnitude of the K_e = 2 curve is unity when $\omega \approx 78$ rad/s. Extrapolation of the phase curves at the $-\pi$ crossing point yields an approximate value for the limiting value of delay as $\tau \approx 0.026$ s. In comparison, the HS scheme can be shown to be unstable if $(m_2/m_1) \geq 1$ when $\tau > 0$ s, or if $(m_2/m_1) < 1$ when $\tau > \tau_c$, where $\tau_c \approx 0.023$s when parameters are set to their nominal values.

For sufficiently high values of ω, (*i.e.* ω > 50 rad/s), an approximation can be made for the magnitude of H in order to determine a solution for the onset of stability. Hence, when ω^2 dominates all other parameters, the magnitude of H in equation (16) can be approximated as $|H(j\omega)| \approx maK_e / (m_1\omega)$, so at the point of instability $\omega = maK_e / m_1$. The corresponding phase relationship then yields the critical value of τ for instability as:

$$\tau \approx \left(m_1 / maK_e \right) \left[\pi - \tan^{-1}\left(mK_e / m_1 \right) \right] \tag{17}$$

Rearrangement of equation (17) generates an iterative solution to the critical value of K_e, as follows:

$$K_e^l = \left(m_1 / ma\tau \right) \left[\pi - \tan^{-1}\left(mK_e^{l-1} / m_1 \right) \right];\ l = 0, 1, 2, \cdots \tag{18}$$

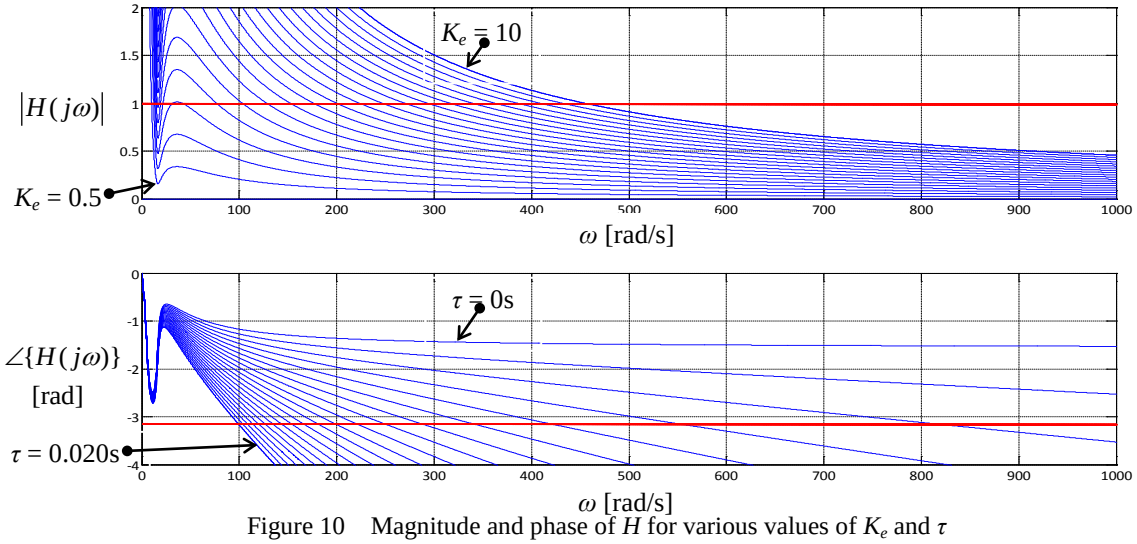

Figure 10 Magnitude and phase of H for various values of K_e and τ
(note that magnitude is independent of τ and phase is independent of K_e)

Returning to the first of the above examples, when τ = 0.003 s, equation (18) yields a steady-state critical gain K_e = 12.01 (to 4 significant figures); this is after 4 iterations and with an initial condition

$K_e^{\,0} = 0$. Clearly, the approximation for critical K_e is close to that obtained from the graphical method. Similarly, the computed value for the critical frequency is $\omega = maK_e / m_1 = 549.5$ rad/s, which is close to the graphical solution of ~550 rad/s.

5. Experimental studies on the QP pilot rig, with (i) LSC and (ii) LSC plus adaptive control

This section describes some representative experimental studies that have been conducted on the QP pilot rig, with an emphasis on the effects of parameter uncertainty and variation. §5.1 focuses on the performance of LSC alone and §5.2 demonstrates how the addition of a parallel adaptive controller, minimal control synthesis with error feedback [1], [8], can improve the DSS synchronization error response still further.

5.1. Experimental studies with linear substructuring control (LSC)

Tests on the QP rig were conducted with all parameters set to their nominal values, save for the parameter under investigation. Hence, with the vehicle velocity maintained at 100 km/h, the resulting parametric excitation due to the variation of stiffness, k_1, is shown in figure 11. The time range for tests was maintained at 30 s throughout the investigations.

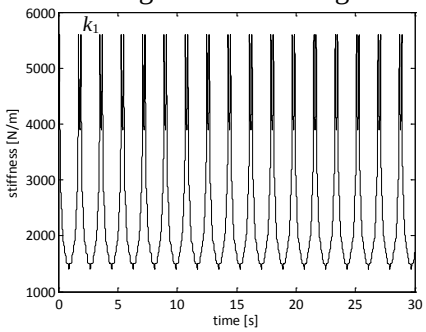

Figure 11 Catenary stiffness k_1; vehicle velocity v = 100 km/h

The first test results are used to compare the effects of variation in the LSC feedback gain K_e. For the nominal case $K_e = 2$, Σ_N and Σ_P responses (y_1 and y_2, respectively) are shown in figure 12(a), together with the corresponding synchronisation error in figure 12(b). Visually, the responses demonstrate excellent synchronisation of the substructure displacements, with the root-mean-square (RMS) of error being computed as 0.0426 mm over an operating range of ~ 6 mm.

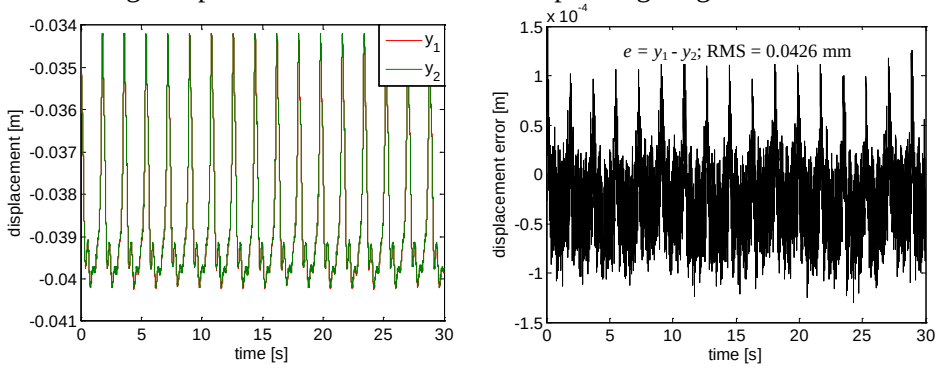

(a) (b)

Figure 12 LSC responses. (a) Numerical (y_1) and physical (y_2) substructure displacements; $K_e = 2$ (nominal)
(b) Corresponding synchronisation error, $e = y_1 - y_2$

Comparison of the above results is enhanced by the use of an integral-square-error (ISE) measure. Thus, figure 13(a) shows the ISE generated by the error response in figure 12(b). Figure 13(b) shows ISE curves for the three cases $K_e = \{1, 2, 3\}$ and, as might be expected, an increase in gain results in smaller errors, smaller ISE amplitudes and smaller RMS values ({0.0635, 0.0426, 0.0360} mm, respectively). This trend does not continue indefinitely, due to signal noise propagation at higher values of K_e and then ultimate instability due to the 0.003 s pure delay in Σ_{TS}.

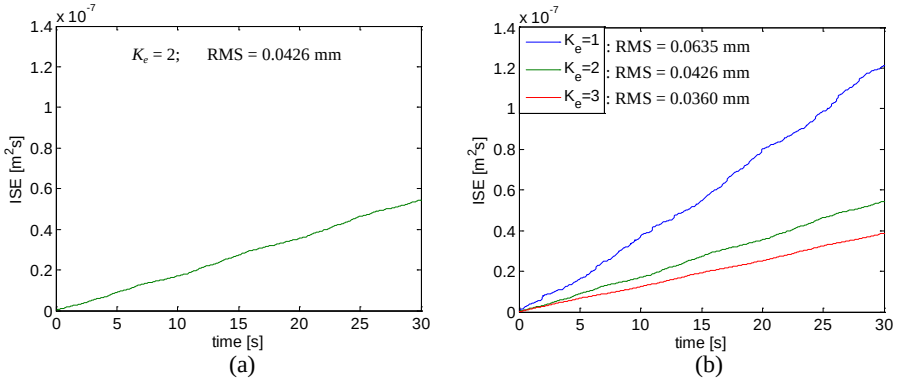

(a) (b)

Figure 13 LSC ISE curves. (a) K_e = 2 (nominal); (b) K_e = {1, 2, 3}

Similarly, tests on c_1 (within Σ_N) result in the LSC responses shown in figures 14 and 15. The nominal results, for c_1 = 500 Ns/m, are shown in figures 14 and 15(a). Again, the synchronisation response is of excellent quality and the RMS value (0.0424 mm) is virtually identical to that from the nominal response obtained previously. Introducing parameter variations for the three cases c_1 = {250, 500, 1000} Ns/m results in the ISE curves of figure 15(b), which have corresponding RMS values of {0.0749, 0.0424, 0.0283} mm. Again, an increase in the parameter tends to improve responses, but this is limited by sluggish closed-loop responses as c_1 approaches very high values.

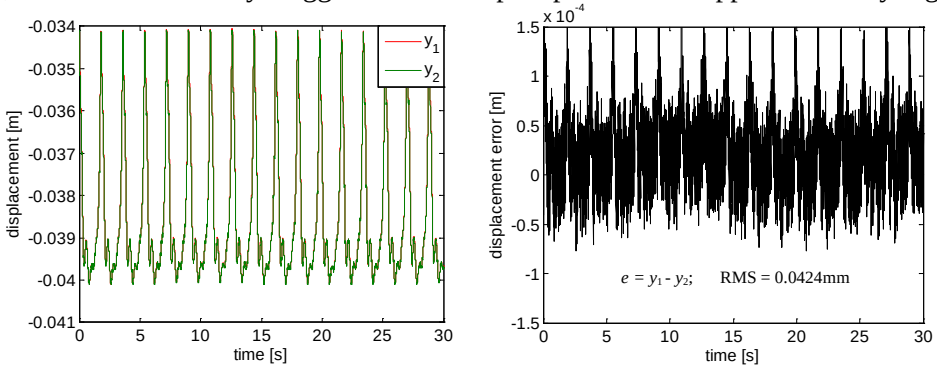

(a) (b)

Figure 14 LSC responses. (a) Numerical (y_1) and physical (y_2) substructure displacements; c_1 = 500 Ns/m (nominal) (b) Corresponding synchronisation error, $e = y_1 - y_2$

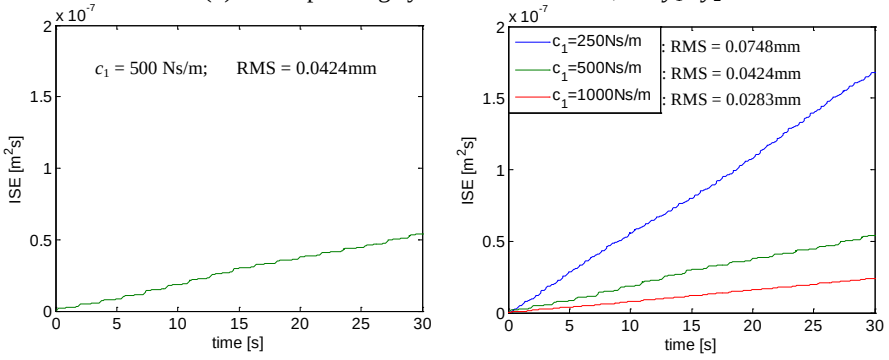

(a) (b)

Figure 15 LSC ISE curves. (a) c_1 = 500 Ns/m (nominal); (b) c_1 = {250, 500, 1000} Ns/m

5.2. Experimental studies with LSC plus adaptive control

Direct adaptive control in the form of the minimal control synthesis with error feedback (MCSEF) algorithm can be used to augment LSC in a straightforward manner [1]. Essentially, the MCSEF algorithm provides an additive component to the control signal generated by LSC and, as a consequence, the adaptive algorithm is located within the outer-loop controller box shown in figure 7(a). A brief summary of MCSEF follows; full details can be found in [1]. The additive

adaptive control signal is given by the following (*c.f.* equation (5)):

$$u_a = K_{1e}(t)d_{e1'} + K_e(t)e \tag{19}$$

so that $u \rightarrow u + u_a$, where the time-varying adaptive gains are:

$$K_{1e}(t) = \alpha\int_0^t \left(y_e d_{e1'}\right)dt + \beta y_e d_{e1'};\ K_e(t) = \alpha\int_0^t \left(y_e e\right)dt + \beta y_e e;\ \{K_{1e}(0^-) = K_{1e0};\ K_e(0^-) = K_{e0}\} \tag{20}$$

Here, α and β are scalar adaptive weights, where α is selected empirically to yield a compromise between adaptive effort and signal noise suppression, $\beta = \alpha/10$ and the initial conditions $\{K_{1e0}, K_{e0}\}$ are chosen as zero. The term $y_e = (4e/t_s)$ is a generalised output error, where t_s is the desired settling-time of the adaptive process. In the tests described below, adaptive parameters were chosen as $\alpha = 10^{-7}$ and $t_s = 0.02$ s; the relatively low value of α in this case is a consequence of scaling within the DSS loop (*e.g.* the magnitude of K_{1e}, is typically ~ -90dB or ~ 3×10^{-5} in normal units).

Figure 16 shows the LSC+MCSEF responses for the parameter-varied case $K_e = 1$. Figure 16(b) details the synchronisation error resulting from the responses in figure 16(a), which has an RMS value of 0.0246 mm, compared with the LSC-only RMS value of 0.0635 mm. This implies an approximately 2.6-fold improvement due to the action of the adaptive controller. On comparing the $K_e = 1$ ISE curve resulting from the action of LSC in figure 13(b) with the LSC+MCSEF result in figure 17(b), an approximately 6.7-fold improvement is evident; (the difference in performance measure ratios is due to the 'extra square' within the ISE calculation).

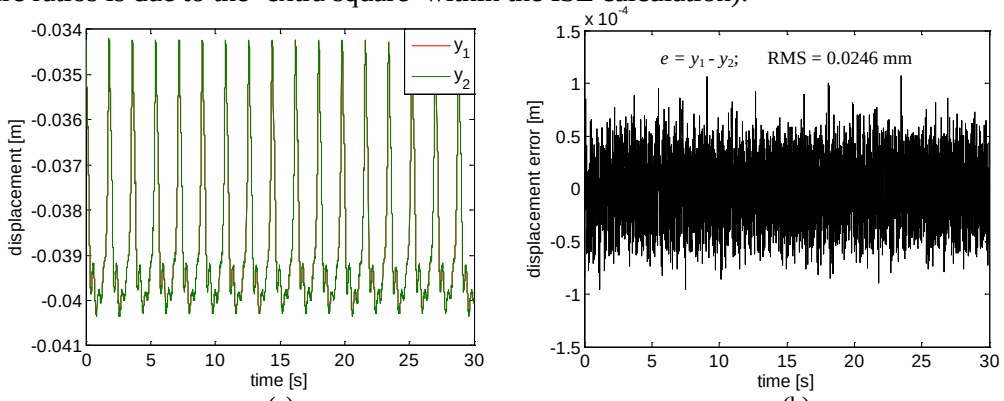

Figure 16 LSC+MCSEF responses when $K_e = 1$ in LSC and $\{\alpha = 10^{-7}, t_s = 0.02$ s$\}$ in MCSEF.
(a) Numerical (y_1) and physical (y_2) substructure displacements (b) Corresponding synchronisation error, $e = y_1 - y_2$

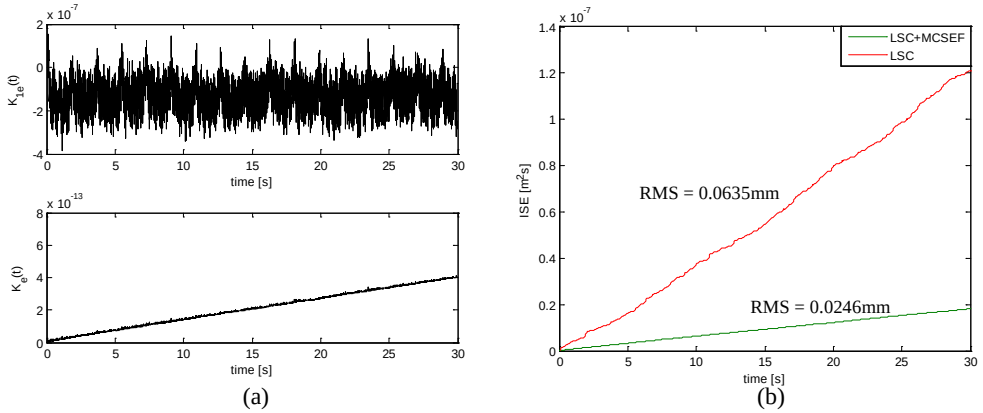

Figure 17 (a) MCSEF adaptive gains: K_{1e} (top) and K_e (bottom) when $K_e = 1$ and $\{\alpha = 10^{-7}, t_s = 0.02$ s$\}$
(b) LSC and LSC+MCSEF ISE curves when $K_e = 1$ and $\{\alpha = 10^{-7}, t_s = 0.02$ s$\}$

6. Conclusions and further work

The main conclusions to this work are summarized as follows:

- The principal contribution of this paper has been to take a first step in the development of a

practical dynamically substructured system (DSS) for the testing of railway vehicle pantographs.

- Simplified substructures were developed for this specific application, with the numerical substructure representing the catenary and the physical substructure representing the pantograph.
- Parametric excitation was included in the formulation as the principle driver for the DSS.
- Linear substructuring control (LSC) yielded excellent synchronisation of substructure displacements, with RMS errors of less than 0.1 mm when the output range was ~6 mm.
- Classical control engineering techniques (roots' loci, Bode plots and Nyquist stability theory) were used to develop LSC and to investigate stability and robustness issues due to parametric uncertainty. LSC was found to be robust in the face of uncertainty of all key parameters, including pure delays in the discrete-time elements of the control and data acquisition hardware.
- Adaptive minimal control synthesis with error feedback (MCSEF) was investigated as an additive parallel component to LSC. MCSEF was found to improve root-mean-square (RMS) errors still further, typically producing a ~3 fold improvement in terms of RMS and ~7 fold in terms of integral-square error (ISE), when compared with the use of LSC alone.

Further development of this work will include the following items:

- Enhancement of the DSS feedback term $K_e(s)$ via pole-zero cancellation methods.
- Incorporation of (nonlinear) finite element models (FEM) within the numerical substructure of the DSS. Conceptually, an FEM will be used in its full-order form within the numerical substructure, but in reduced-order form in the synthesis of DSS synchronizing controller(s). A promising preliminary study of this approach is described in [9], using the DSS method as a basis for implementation. It can be noted that the proposed reduced-order FEM approach is an alternative to the modal superposition method of [10] and the method described in [11].
- Synthesis of a state-space description of the proposed FEM-based DSS.
- Experimental verification of the FEM-based DSS, including development of the physical substructure via the use of a standard pantograph mechanism.
- Comparison of the above with existing hybrid simulation (HS) testing results.
- Analysis and test of contact and impact problems between the catenary and pantograph.

References

[1] Stoten DP and Hyde RA 2006 Adaptive control of dynamically substructured systems: the single-input single-output case *Proc. IMechE, Part I: J. Systems and Control Eng.* **220** 2 pp63-79.
[2] Magonette G 2001 Development and application of large-scale continuous pseudo-dynamic testing techniques *Phil. Trans. R. Soc. Lond.* A **359** pp1771-99.
[3] Nakashima M, Kato H and Takaoka E 1992 Development of real-time pseudo dynamic testing *Earthquake Engng. Struct. Dyn.* **21** 1 pp1121-41.
[4] Horiuchi T, Inoue M, Konno T and Namita Y 1999 Real-time hybrid experimental system with actuator delay compensation and its application to a piping system with an energy absorber *Earthquake Engng. Struct. Dyn.* **28** 10 pp80-92.
[5] Brandt EP, Wang Y and Grizzle JW 1997 A simplified three-way catalyst model for use in on-board SI engine control and diagnostics *Proc. ASME Dynamic Systems and Control* pp 653-9.
[6] Raman S, Sivashankar N, Milam W, Stuart W and Nabi S 1999 Design and implementation of HiL simulators for powertrain control system software development *Proc. ACC.* pp709-13.
[7] Stoten DP 2014 A comparison of hybrid and DSS schemes for substructured system testing *MOVIC 2014 – 12th Int. Conf. Motion and Vibration Control* Japan Soc. Mech. Eng. Hokkaido Japan.
[8] Stoten DP, Tu J-Y and Li G 2009 Synthesis and control of generalized dynamically substructured systems *Proc. IMechE, Part I: J. Systems and Control Eng* **223** pp371-92.
[9] Yamashita Y, Usuda T and Kobayashi S 2015 Application of dynamically substructured systems scheme to parametric excitation system intended to HILS test procedure for catenary pantograph system *Proc. 22nd United Symp. Railway Tech.* Japan Soc. Mech. Eng. Tokyo Japan.
[10] Facchinetti A, Gasparetto L and Bruni S 2013 Real-time catenary models for the hardware-in-the-loop simulation of pantograph-catenary interaction *Vehicle System Dynamics* **51** 4 pp499-516.
[11] Ikeda M 2015 'Gasen-do FE' statement of methods *Vehicle System Dynamics* **53** 3 pp357-69.